Journal of Signal Processing, Vol.23, No.4, pp.201-204, July 2019

SELECTED PAPER AT NCSP'19

# Autonomous Traveling Control of Agricultural Mobile Robot Using Depth Camera in Greenhouse

Satoshi Yamashita, Hiroshi Suzuki, Akinobu Kuwahara,
Takahiro Kitajima and Takashi Yasuno

Graduate School of Advanced Technology and Science, Tokushima University
2-1 Minami-Josanjima, Tokushima 770-8506, Japan
E-mail: yamashita-s@ee.tokushima-u.ac.jp
{suzuki.hiroshi, yasuno.takashi} @tokushima-u.ac.jp

**Abstract**

We describe traveling control of an agricultural mobile robot using a depth camera in a greenhouse. In our previous research, we also developed an agricultural mobile robot using a 2D laser range finder (2D-LRF). However, since the detection area of the 2D-LRF is only a 2D plane at the installation height, it is difficult to classify the type of obstacles using the 2D-LRF. On the other hand, the depth camera can detect distances in 3D space and capture 2D color images. For that reason, we propose an autonomous traveling control algorithm for the robot using the depth camera. Depth information output from the depth camera is converted to 2D data and the robot is controlled on the basis of the 2D-LRF algorithm. Several experimental results using our developed mobile robot in a mock-up greenhouse demonstrate the usefulness of the proposed control algorithm using the depth camera.

## 1. Introduction

In recent years, it has been necessary to improve both quality and yield in agriculture because consumers tend to choose higher quality crops, and high productivity is needed to maintain business in the agricultural field. Therefore, large-scale greenhouses are attracting attention and being rapidly introduced. However, there is a problem that the burden of agricultural workers is increasing owing to the decrease in the working population. To solve this problem, the introduction of agricultural robots that can work automatically is expected. Therefore, various types of agricultural robot are currently being researched and developed. In our previous research, we also developed an agricultural mobile robot using a 2D laser range finder (2D-LRF)[1].

For a robot to perform several tasks such as pesticide spraying and harvesting, autonomous traveling along side crops is one of the fundamental functions. Although the 2D-LRF is useful in detecting obstacles surrounding the traveling robot, the detection area is only a 2D plane at the installation height. Therefore, it is difficult to classify obstacles such as leaves of crops, walls, agricultural equipment and workers using the 2D-LRF. On the other hand, the depth camera can detect distance in 3D space, capture 2D color images and is available at a low cost. Therefore, it is possible to compensate for the disadvantage of the 2D-LRF by using the depth camera.

In this paper, we propose an autonomous traveling control algorithm for a robot using the depth camera. The tested depth camera is mounted on the front of the robot and detects obstacles and passageways in 3D space. Depth information output from the depth camera is converted to 2D data to input adapted to the 2D-LRF algorithm. The left and right driving wheels are controlled independently on the basis of information from the depth camera and the 2D-LRF. Several experimental results using our developed mobile robot in a mock-up greenhouse demonstrate the usefulness of the proposed control algorithm using the depth camera.

## 2. Agricultural Mobile Robot

Figure 1 shows the appearance of the agricultural mobile robot developed for the purpose of harvesting and pesticide spraying. The carrier of the robot is flat so that a harvesting module or spraying module can be mounted. The specifications of the robot are listed in Table 1. The size of the robot was decided taking into consideration the traveling lane width of a typical large-scale greenhouse. The 2D-LRF and the depth camera are mounted at the front of the robot. The robot has rear two wheels driven by motors and two free casters at the front. The reference speed of each motor is calculated from the surrounding information measured by the 2D-LRF and the depth camera.

Figure 2 shows the hardware system configuration of the robot. A PC is mounted on the robot to control the motors in accordance with the information on the surroundings.

The specifications of the 2D-LRF and the depth camera are listed in Table 2. The 2D-LRF measures the distance by the


**Figure 1:** Developed agricultural mobile robot

**Table 1:** Specifications of developed robot

| | |
|---|---|
| Size | 540 (W) × 780 (L) × 1090 (H) mm |
| Depth camera | Intel RealSense Depth Camera D435 |
| 2D-LRF | HOKUYO UST-10LX |
| Motor | Nissei, VHLD28L/R-20N400L2 |
| Battery | Lithium ion 24 V, 36 A<br>NiMH 24 V, 20 Ah |

time of flight (ToF) method, in which the distance is measured by measuring the flight time of reflected light from the target object. The 2D-LRF can measure the distance on a certain plane by rotating the mirror used for scanning. The depth camera uses the active infrared (IR) stereo method to measure the projected IR laser pattern from the IR laser projector using left and right IR cameras, and calculates the distance on the basis of stereo vision. The depth camera outputs depth data calculated between obstacles and a vertical plane on the front surface of the image sensor. Figures 3(a) and 3(b) respectively show a color image and a depth image obtained by the depth camera. The depth image shows the depth data as a gradation of colors from red to blue. A disadvantage of the depth camera is that depth data cannot be acquired in the area where visual fields do not overlap, mainly on the left side of the subject, as shown in Fig. 3(b). A region where depth data cannot be obtained is expressed as zero.

Although the 2D-LRF is useful in detecting obstacles surrounding a traveling robot, the detection area is only the 2D plane at the installation height. Therefore, the 2D-LRF cannot detect obstacles at other heights. Moreover, it is difficult to classify obstacles such as leaves of crops, walls and agricultural equipment using the 2D-LRF. Hence, there is a possibility of collision with crops of a height undetectable by the 2D-LRF or erroneous operation due to misrecognition of walls and obstacles. On the other hand, the depth camera can detect the horizontal distance from obstacles in 3D space and capture 2D color images. However, the depth camera has an angle of view of only $91.2^\circ$, which is $1/3$ that of the 2D-LRF, and depth data contains a large amount of noise. In addition, since the depth camera handles more data than the 2D-LRF, a longer processing time is required. Therefore, to use the depth camera for traveling control, it is necessary to remove noise and reduce the calculation cost.

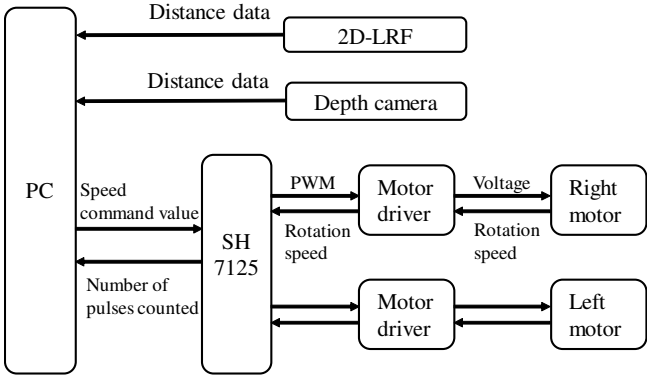


**Figure 2:** Hardware system configuration

**Table 2:** Specifications of 2D-LRF and depth camera

| | 2D-LRF | Depth camera |
|---|---|---|
| Product name | UST-10LX | Intel RealSense<br>Depth Camera D435 |
| Measurement method | ToF | Active IR stereo |
| Detection range | 0.06 – 10 m | 0.2 – 10 m |
| Angle range | 270°<br>(Horizontal) | 91.2°, 65.5°, 100.6° (±3°)<br>(Horizontal, vertical, diagonal) |
| Scanning time | 25 ms | Max 90 fps |
| Resolution | 0.25° | 1280 × 720 |

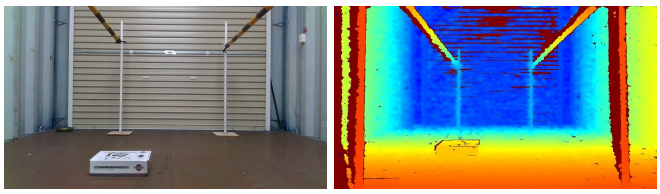

**(a)** Color image **(b)** Depth image

**Figure 3:** Data obtained from depth camera

## 3. Processing Algorithm of Depth Data

In this paper, we convert 3D depth data to 2D data compatible with the 2D-LRF and apply it to conventional travel algorithms for the 2D-LRF. The conversion process to 2D data consists of ground detection, noise removal and data dimension reduction.

### 3.1 Ground detection

As shown in Fig. 3(b), the depth camera equally measures the ground and obstacles. The distance to the ground is recognized as the nearest obstacle in many cases. Therefore, it is necessary to remove the depth data measured for the ground. For ground detection, we applied the step extraction method using a 3D sensor proposed by Eguchi and Ozaki[2]. In this method, the robot retains prior measurement data of the flat ground and compares it with the current measurement data, thereby detecting any irregularity of the ground such as a step. On the upper step, as shown in Fig. 4, the measured depth $z$ becomes smaller than the depth $Z$ along the flat ground owing to the height difference. Therefore, when $z > \alpha Z$ $(0 < \alpha \leq 1)$, the measured position is judged to be the ground. In this work, we set $\alpha$ to 0.95. Figure 5 shows the depth image when the depth of the measured position detected as a passage is set to dark blue.

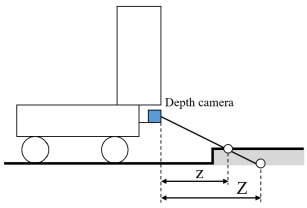


**Figure 4:** Upper step detection

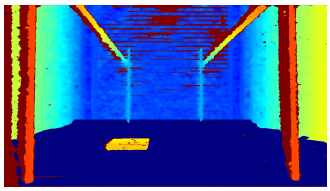

**Figure 5:** Depth image after removal of ground

### 3.2 Noise removal

Figures 6(a) and 7(a) respectively show the depth image and the result after conversion to 2D data before noise removal. Noise occurs at places where depth data cannot be obtained. Such noise occurs as a result of the misinterpretation that there are obstacles in places without measurement values. Therefore, the area surrounded by pixels having a depth of zero was checked, and when such an area is less than 20 pixels in height and width, it is judged to be noise and is removed. The area is obtained using a Freeman chain code. As a result, it is confirmed that noise is removed, as shown in Fig. 6(b), and the depth image is correctly converted to 2D data, as shown in Fig. 7(b). However, as shown in Fig. 6(b), obstacles that should not be removed have been partially removed.

### 3.3 Data dimension reduction

Too much processing time is required to use the 3D depth data output from the depth camera for traveling control. Therefore, to shorten the processing time, the depth data is converted from 3D data to 2D data. First, the minimum depth data other than zero is extracted from each column of the depth image and stored in a 1D array with the number of elements equal to the width of the image. After that, the coordinate on the x-axis of element position $x_p$ is obtained as

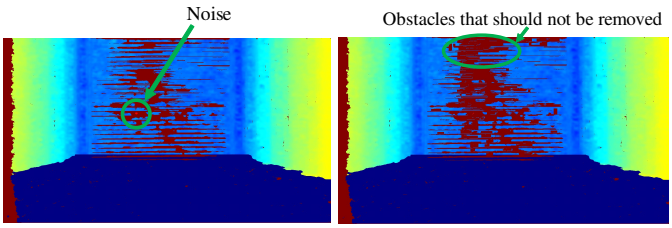


**(a)** Before **(b)** After

**Figure 6:** Results of noise removal from depth image

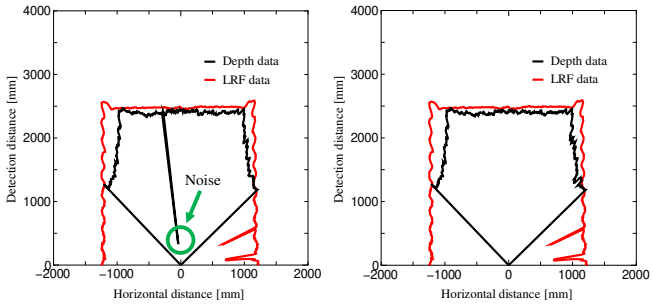


**(a)** Noise detection **(b)** Noise removal

**Figure 7:** Results after converting the depth image to 2D data

$$x_p = z_p \tan\left(\frac{x - w/2}{w/2} \times \frac{\theta_{\max}}{2}\right) \tag{1}$$

where $x$ is the x-axis position in the image, $z_p$ is the depth data of the element, $w$ is the image width and $\theta_{\max}$ is the horizontal viewing angle of the depth camera. The result of conversion from the depth image of Fig. 3(b) to 2D data is shown in Fig. 8. The depth camera detects the box and pipes that cannot be detected by 2D-LRF because of their location height.

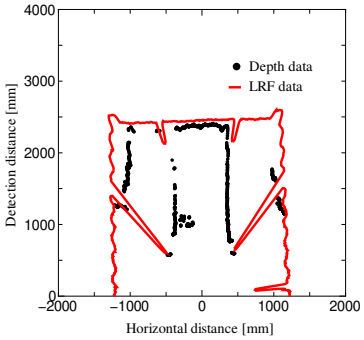


**Figure 8:** Results of converting 3D depth data to 2D data in the same situation as shown in Fig. 3(a)

## 4. Traveling Experiments

We evaluated the obstacle avoidance performance using the depth camera in a mock-up greenhouse with crops that cannot be detected by the 2D-LRF. The usefulness of the depth camera was verified by the result of traveling experiments in the mock-up greenhouse. The method of combining 2D-LRF and depth camera data during control yields the shortest distance from the two sets of data and applies it to the traveling algorithm.

Figures 9(a) and 9(b) respectively show an overview and the dimensions of our test course. The height of the crop is set higher than 30 cm from the ground.

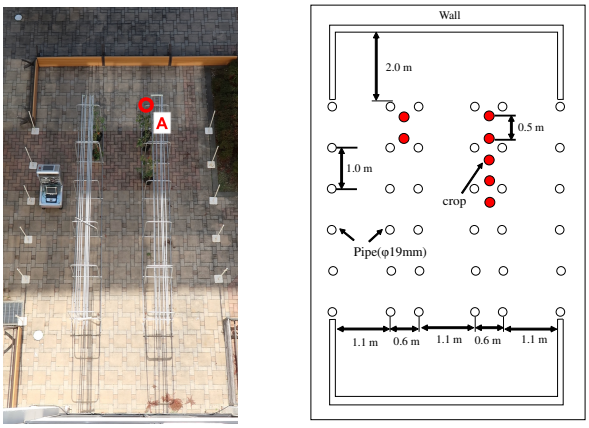


**(a)** Overview **(b)** Structural layout including dimensions

**Figure 9:** Test course for experiments

### 4.1 Avoidance of crops between the plant bed

Figures 10(a) and 10(b) respectively show the traveling results for a straight passage using only the 2D-LRF and the depth camera with the 2D-LRF. As shown in the figure, the robot travels a meandering path to detect a pot in which crops are planted. However, because crops cannot be detected, collision with the crops occurs at $t = 13$ s. On the other hand, as shown in Fig. 10(b), it can be confirmed that the robot using the depth camera travels while avoiding the crops.

### 4.2 Approaching a passage with protruding crops

Figures 11(a) and 11(b) respectively show the traveling results for a corner and approaching a passage using only the 2D-LRF and the depth camera with the 2D-LRF. In the current traveling algorithm, the robot turns toward the passage after approaching close enough to point A in Fig. 9(a), the edge of the plant bed, to enter passage between plant beds. Therefore, as shown in Fig. 11(a), the robot collides with crops on the edge at $t = 30$ s. On the other hand, as shown in Fig. 11(b), by using the depth camera, it can be confirmed that the robot travels without collision with the crops at $t = 30$ s. However, just before entering the passage between the plant

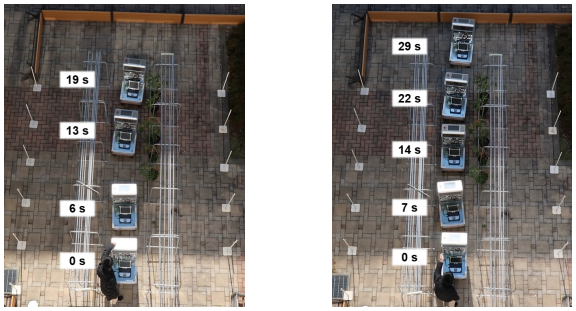


**(a)** 2D-LRF **(b)** 2D-LRF and depth camera

**Figure 10:** Trajectory when traveling between plant beds

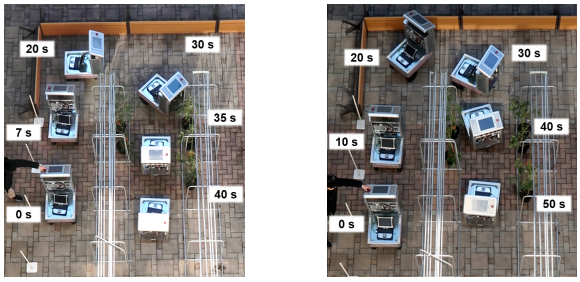


**(a)** 2D-LRF **(b)** 2D-LRF and depth camera

**Figure 11:** Trajectory when entering passage between plant beds

beds, collision occurred with the crops on the inside of the turn, which is a blind spot of the depth camera.

## 5. Conclusions

In this paper, we proposed an autonomous traveling control algorithm for a robot using a depth camera. It was confirmed that the robot can detect and avoid crops at various heights when using the depth camera. However, there were cases where the robot collided with crops located outside the angle of view detectable by the depth camera. As a future task, to reduce collisions with crops outside the detection range of the depth camera, we must add an algorithm for memorizing position information of obstacles detected in the past.

## References

[1] N. Nakao, H. Suzuki, T. Kitajima, A. Kuwahara and T. Yasuno: Path planning and traveling control for pesticide-spraying robot in greenhouse, Journal of Signal Processing, Vol. 21, No. 4, pp. 175-178, 2017.

[2] J. Eguchi and K. Ozaki: Extraction method of travelable area by using of 3D-laser scanner —Development of autonomous mobile robot for urban area—, Transactions of the Society of Instrument and Control Engineers, Vol. 52, No. 3, pp. 152-159, 2016.